OPEN ACCESS
CellPress

Cell Reports
Resource

Functional Genomic Analysis of Human Mitochondrial RNA Processing

Ashley R. Wolf[1,2,3] and Vamsi K. Mootha[1,2,3,*]
[1]Howard Hughes Medical Institute, Department of Molecular Biology, and Center for Human Genetic Research, Massachusetts General Hospital, Boston, MA 02114, USA
[2]Department of Systems Biology, Harvard Medical School, Boston, MA 02115, USA
[3]Broad Institute, Cambridge, MA 02141, USA
*Correspondence: vamsi@hms.harvard.edu
http://dx.doi.org/10.1016/j.celrep.2014.03.035

SUMMARY

Both strands of human mtDNA are transcribed in continuous, multigenic units that are cleaved into the mature rRNAs, tRNAs, and mRNAs required for respiratory chain biogenesis. We sought to systematically identify nuclear-encoded proteins that contribute to processing of mtRNAs within the organelle. First, we devised and validated a multiplex MitoString assay that quantitates 27 mature and precursor mtDNA transcripts. Second, we applied MitoString profiling to evaluate the impact of silencing each of 107 mitochondrial-localized, predicted RNA-binding proteins. With the resulting data set, we rediscovered the roles of recently identified RNA-processing enzymes, detected unanticipated roles of known disease genes in RNA processing, and identified new regulatory factors. We demonstrate that one such factor, FASTKD4, modulates the half-lives of a subset of mt-mRNAs and associates with mtRNAs in vivo. MitoString profiling may be useful for diagnosing and deciphering the pathogenesis of mtDNA disorders.

INTRODUCTION

Human mtDNA encodes 13 protein subunits of the respiratory chain, as well as the two rRNAs and 22 tRNAs required for their translation. All protein factors that are required for mtDNA replication, transcription, and translation are nuclear encoded and imported into the mitochondrion. Mutations in either nuclear- or mitochondrial-encoded genes cause a range of heritable disorders with overlapping phenotypes. Expression of nuclear- and mtDNA-encoded oxidative phosphorylation (OXPHOS) complex proteins is coordinated by nuclear transcription factors and coactivators (Scarpulla et al., 2012). However, local control of mtDNA expression is also possible, as suggested by the finding that chemical perturbations are capable of decoupling the expression of the two genomes (Wagner et al., 2008).

The 16.5 kB human mitochondrial genome is highly compact and transcribed by mtRNA polymerase as two continuous polycistrons, one for each strand. The "heavy strand" expresses two rRNAs, 14 tRNAs, and 12 mRNAs, while the "light strand" expresses the *ND6* mRNA and eight tRNAs (Figures 1A and 1B). These precursor RNAs primarily contain mt-mRNAs "punctuated" by tRNAs, whose structure is proposed to guide the cleavage responsible for liberating individual mt-mRNAs and tRNAs (Anderson et al., 1981; Ojala et al., 1981). Cleavage at the 5′ end of tRNAs is catalyzed by the RNase P complex, which is comprised of three recently identified proteins: mitochondrial RNase P protein 1 (MRPP1), MRPP2, and MRPP3 (Holzmann et al., 2008). An alternative RNase P containing an imported catalytic RNA has also been described (Puranam and Attardi, 2001). Cleavage at the 3′ end of tRNAs is catalyzed by the nuclease ELAC2 (Brzezniak et al., 2011; Sanchez et al., 2011). After cleavage, the mtRNA poly-A polymerase (MTPAP) polyadenylates the mt-mRNAs (Nagao et al., 2008; Piechota et al., 2006). mt-mRNA abundance is regulated by the SLIRP- LRPPRC complex, although the exact mechanism is debated. LRPPRC has been implicated in mt-mRNA transcription, polyadenylation, translation, and degradation suppression (Baughman et al., 2009; Chujo et al., 2012; Gohil et al., 2010; Liu et al., 2011; Ruzzenente et al., 2012; Sasarman et al., 2010).

Despite the concurrent transcription of heavy-strand genes, their cognate mt-mRNAs reach distinct steady-state levels. These ten transcripts have distinct half-lives that fall into two categories: short-lived and long-lived. The complex I transcripts *ND1–ND3* and *ND5*, and the complex III transcript *CYTB* are short-lived ($\tau_{1/2}$ = 68–94 min), whereas the complex IV transcripts cytochrome *c* oxidase 1 (*COX1*), *COX2*, and *COX3*; complex V bicistronic transcript *ATP6/8*; and complex I bicistronic transcript *ND4/4L* are long-lived ($\tau_{1/2}$ = 138–231 min) (Nagao et al., 2008). These differential mt-mRNA stabilities are consistent with early observations (Gelfand and Attardi, 1981) and recent RNA-sequencing analysis (Mercer et al., 2011), but remain unexplained by transcript length, polyadenylation, known degradation pathways, or characterized stability factors. Although the purpose of these differential half-lives is unexplored, we note that concentrations of OXPHOS protein complexes (reviewed by Lenaz and Genova, 2010) tend to correlate with reported mt-mRNA half-lives (Nagao et al., 2008). Complex I is the least abundant complex and contains

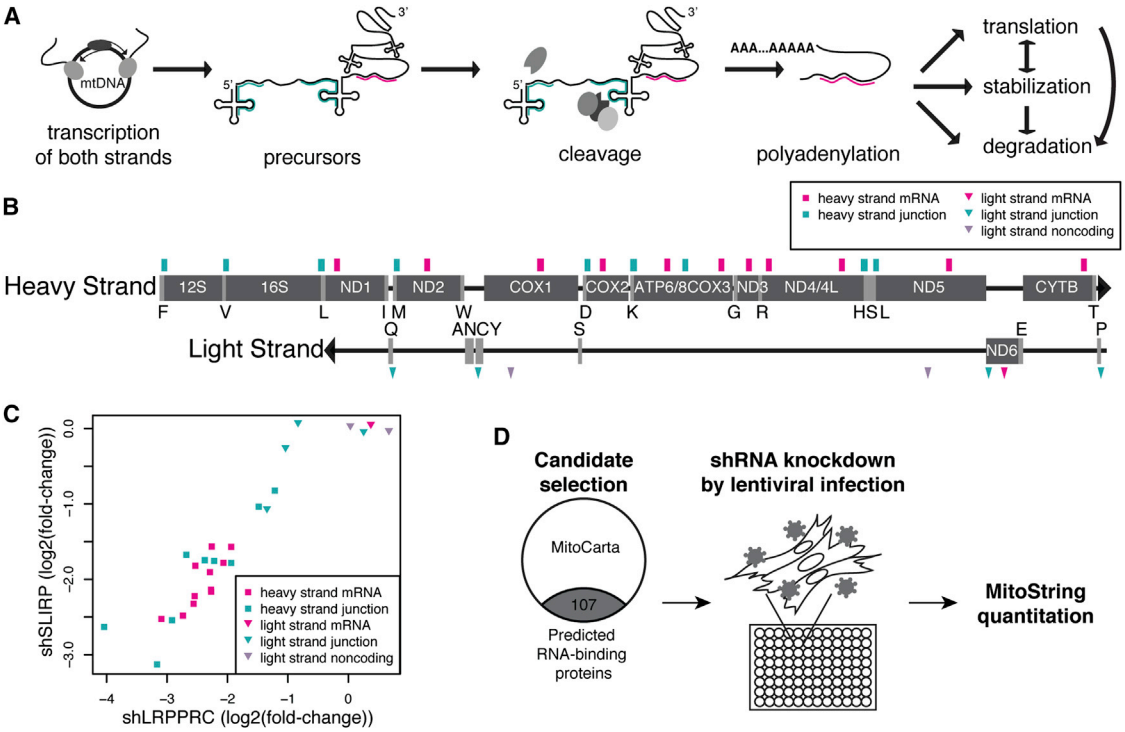

Figure 1. MitoString Screen for Regulators of mtRNA Processing

(A) Schematic depicting mtDNA transcription (in two continuous units, the heavy and light strands) followed by cleavage into individual mRNAs, tRNAs, and rRNAs. Pink and turquoise lines represent MitoString probes targeting mRNAs and junctions, respectively.

(B) Location of MitoString probes on the mtDNA heavy and light strands. rRNAs and mRNAs encoded by the mtDNA are labeled in white text. tRNAs are demarcated by their one-letter symbols. The locations of mRNA, junction, and noncoding probes are denoted in pink, turquoise, and gray, respectively. Rectangles indicate probes targeting the heavy strand, and triangles indicate probes targeting the light strand.

(C) Comparison of the effects of *shLRPPRC* and *shSLIRP* on MitoString probes, shown as log2(fold-change) with respect to *shGFP*. Probe colors and shapes are depicted as in (B).

(D) Overview of the MitoString screening approach. Candidates for lentiviral knockdown were selected by identifying MitoCarta proteins containing RNA-binding domains. Candidate genes were knocked down in WI-38 fibroblasts and the mtRNA levels were assessed 6 days later by the MitoString probes described in (B). See also Figure S1.

subunits encoded by the short-lived mt-mRNAs. Thus, differences in mt-mRNA abundance may help establish OXPHOS protein stoichiometry.

Because all mt-mRNA transcripts but one originate from a single heavy-strand promoter, the observed steady-state levels are expected to be highly dependent on transcript degradation rates (Chujo et al., 2012). The helicase SUPV3L1, in complex with polynucleotide phosphorylase (PNPT1), has been implicated in the degradation of light-strand transcripts, and a dominant-negative form of either gene stabilizes light-strand noncoding transcripts and some short-lived heavy-strand mt-mRNAs (Borowski et al., 2013; Szczesny et al., 2010). However, both RNAi and dominant-negative experiments targeting *SUPV3L1* or *PNPT1* actually decreased the levels of the long-lived mt-mRNA *COX1*, indicating that additional degradation or feedback mechanisms may exist.

Our goal was to systematically identify mitochondrial proteins that contribute to mtRNA processing. We began with a scalable, accurate method to measure multiple mtRNAs throughout the processing stages. Previous approaches for measuring mtRNA levels, such as northern blotting, quantitative PCR (qPCR), and gene expression-based high-throughput screening (GE-HTS; Wagner et al., 2008), have been valuable, but are limited by scalability, strand specificity, or dynamic range, respectively. Here, we report simultaneous, strand-specific measurement of multiple precursor and mature mtDNA-encoded RNAs following stable genetic silencing of nuclear factors predicted to play a role in mtRNA biology. We produced a focused compendium of mtRNA expression across a set of targeted genetic perturbations, which we mined to probe the identity and role of nuclear-encoded factors in mtRNA processing. In the process, we identified *FASTKD4*, a factor that regulates the stability of a subset of mt-mRNAs.

RESULTS

MitoString: A Multiplexed Assay for Precursor and Mature mtRNAs

We developed MitoString assay for interrogating four types of transcripts using the nCounter Analysis System (Geiss et al.,

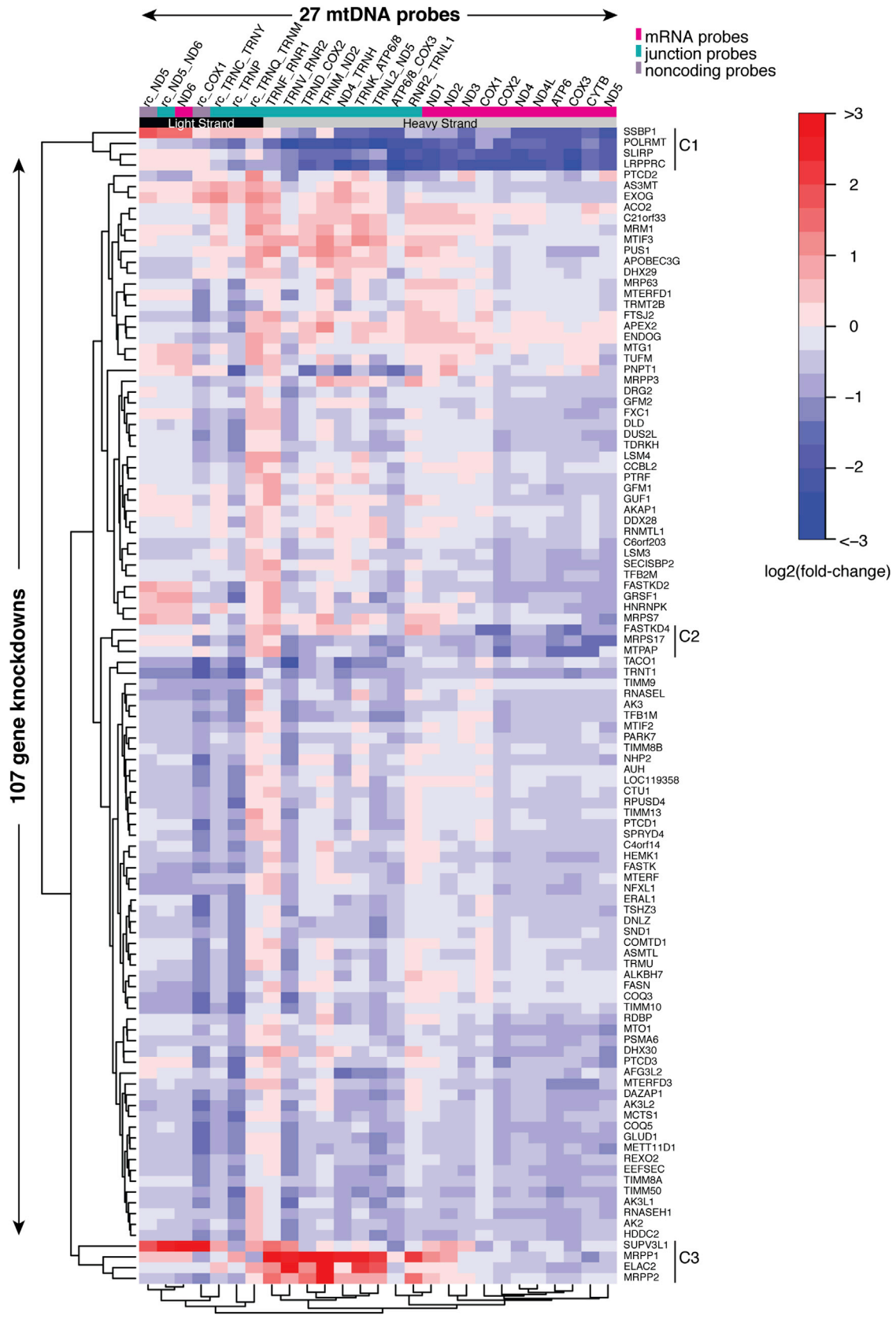

(legend on next page)

2008), in which fluorescent RNA probes quantitate unamplified RNA within a crude cell lysate sample. First, we designed a probe that targets each of the highly abundant mt-mRNA transcripts (Figure 1B), and achieved a coefficient of variation (CV) of 7%–14% for all but one probe across ten independent infections of the control hairpin *shGFP* (Figures S1A and S1B). Second, we designed probes to two regions of the light-strand precursor that are transcribed but are not believed to encode a functional protein. Third, we designed probes that overlap the junctions of two adjacent genes. These junction probes only produce signal when bound to the unprocessed precursor transcript. Probes that assess the precursor strands have lower signal at baseline and thus are noisier (Figure S1C), but their levels can be reproducibly induced in response to perturbation. In addition, we designed probes to detect nuclear-encoded genes that are important for mitochondrial function, as well as nuclear-encoded candidate genes, with the vast majority having a CV of <20% (Figure S1D).

To verify that mtRNA perturbations were measured reliably, we profiled cells following transduction with *PGC-1α*, which induces mitochondrial biogenesis, and *shLRPPRC*, which depletes mtRNAs. *PGC-1α* overexpression increased mature and immature transcripts (Figures S2A and S2B), as well as nuclear-encoded, mitochondrial-localized transcripts (Figure S2C), as expected. *LRPPRC* silencing depleted heavy-strand mt-mRNAs, as found previously (Figure 1C). We further note that knockdowns of the individual components of the LRPPRC-SLIRP complex had well-correlated effects on all transcripts measured by MitoString (Figure 1C), suggesting that hierarchical clustering of MitoString profiles may be valuable for predicting gene function.

Prioritizing Candidate mtRNA-Binding Proteins for Knockdown

With a facile assay for quantifying immature and mature mitochondrial transcripts in hand, we proceeded to select genes that might be involved in mtRNA processing for RNAi-based silencing. We focused on members of MitoCarta, a high-confidence collection of mitochondrial-localized proteins (Pagliarini et al., 2008), and prioritized proteins with known or predicted RNA-binding domains based on Pfam, Gene Ontology (GO) annotation, or manual curation (Figure 1D; Finn et al., 2008). We excluded components of the mitochondrial ribosome and prioritized a total of 107 candidates.

For each of these genes, we selected the three most effective lentiviral short hairpin RNAs (shRNAs) available from the RNAi Consortium (Table S1; Experimental Procedures). We screened WI-38 fetal lung fibroblasts, which are untransformed and viable after 6 days of strong *LRPPRC* knockdown. Cells were infected with hairpins in duplicate and lysed for MitoString analysis after 6 days of antibiotic selection. Using our nuclear NanoString probes, we were able to measure knockdown efficiency for most hairpins within the same assay (Table S2). On each 96-well screening plate, we included five hairpins targeting nonhuman sequences as RNAi controls, a hairpin targeting *LRPPRC* (which is known to deplete mt-mRNAs; Figure 1C), and a *PGC-1α* overexpression construct to stimulate mitochondrial biogenesis (Figures S2A–S2C).

A Compendium of Perturbational Profiles for mtRNA

MitoString quantitation of knockdown perturbations provides a valuable compendium for gene function prediction and mtDNA transcript characterization. Each expression value is normalized to a set of endogenous controls and calculated as a fold change compared with *shGFP*, one of our controls targeting nonhuman sequences. Since *PGC-1α* induction and *LRPPRC* knockdown produce the expected mt-mRNA perturbations (Figures 1C and S2A–S2C), we have confidence that our data set can identify novel regulators. By hierarchically clustering the average perturbational profile across hairpins for each of 107 gene knockdowns along each dimension, we can identify genes and mitochondrial transcripts that may have similar functions (Figure 2; Tables S3 and S4). Unsupervised hierarchical clustering automatically groups *LRPPRC* and *SLIRP* together with *POLRMT*, which encodes the RNA polymerase responsible for mtDNA transcription, and *SSBP1*, which encodes a protein required for mtDNA replication (Figure 2, cluster C1). Separately, genes with roles in mtRNA precursor cleavage, including *ELAC2* and *MRPP1*, also form a strong group based on the signature of junction probe enrichment (Figure 2, cluster C3). Unsupervised hierarchical clustering of the MitoString probes results in automated segregation of light-strand probes, heavy-strand mRNAs, and heavy-strand junctions (Figure 2). Principal component analysis further demonstrates the power of our data set to differentiate these distinct transcript types (Figure S1F). In particular, the heavy-strand junction and mRNA probes are separated by principal component 2, which explains 19% of the variance. The lone mRNA-mRNA junction, *ATP6/8_COX3*, is the sole outlier junction, as it behaves like its mature products, *ATP6/8* and *COX3*. These unsupervised analyses indicate that many genes targeted for RNAi are grouped by function and that mtDNA transcripts respond to perturbations in modules.

Knockdown of *LRPPRC* or *SLIRP* Depletes All Heavy-Strand mtRNAs

By mining the compendium, we gain insight into the action of LRPPRC and SLIRP, which are the strongest regulators tested. Knockdown of *LRPPRC* or *SLIRP* results in depletion of the heavy-strand precursor and all its resulting mt-mRNAs (Figure 2, cluster C1). In addition to *LRPPRC* and *SLIRP*, *POLRMT* and *SSBP1* also universally deplete heavy-strand mtRNAs when

Figure 2. MitoString Profiles for 107 Gene Knockdowns

Heatmap depicts the log2(fold-change) expression level of each of 27 mtDNA probes across 107 gene knockdowns. mtDNA probes are noted along the top and ordered by hierarchical clustering (Euclidean distance). Each gene was targeted by three distinct lentiviral hairpins and measured in duplicate. The mean of all hairpins for a given gene is displayed and the genes are hierarchically clustered (Euclidean distance). Red represents increased expression and blue represents decreased expression with respect to *shGFP*. Identifiers starting with "TRN" denote tRNAs. Probe colors are as described in Figure 1B.
See also Figure S2 and Tables S1, S2, S3, S4, and S5.

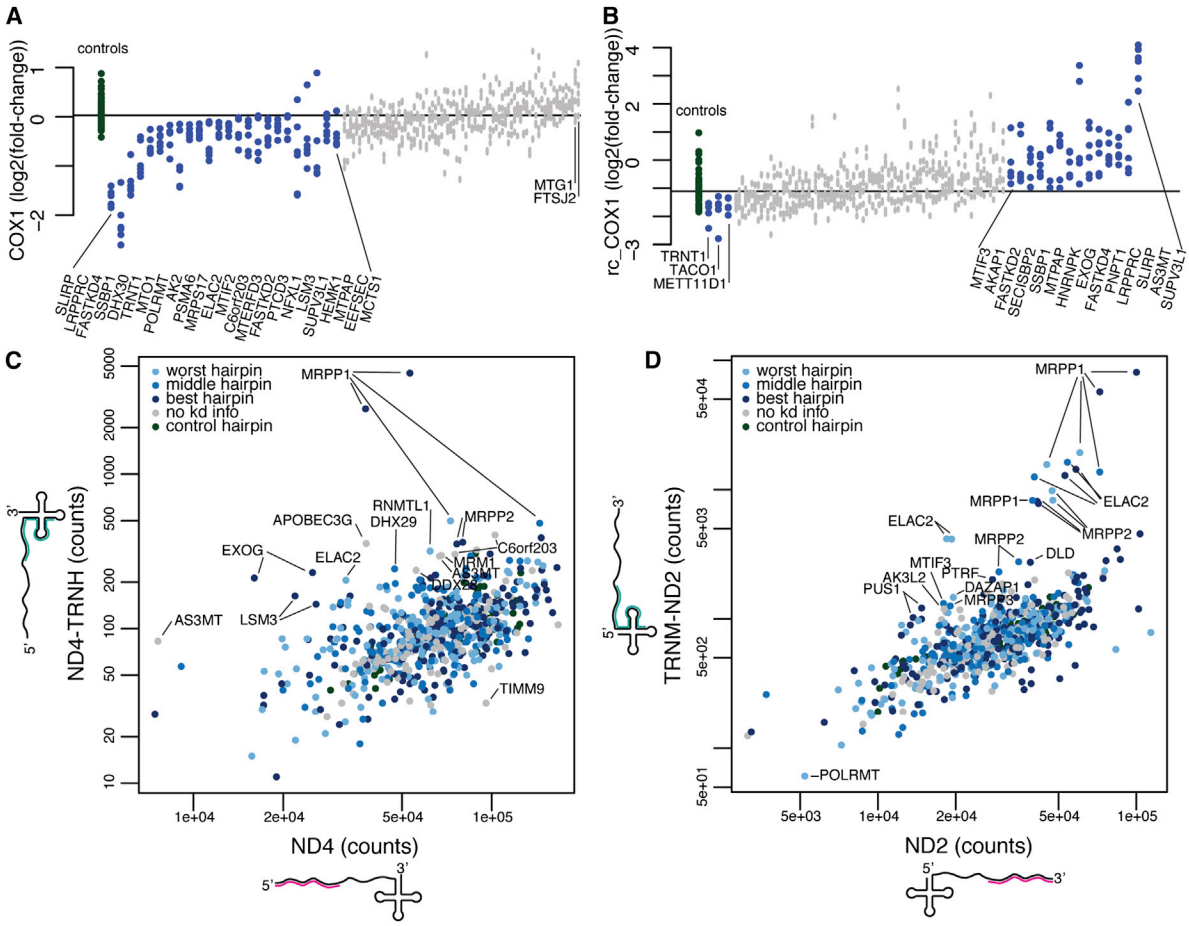

Figure 3. Discordant Expression of Junction and Noncoding Probes Highlights Genes Required for Processing and Degradation

(A) Expression of the *COX1* probe as a log2(expression/*shGFP* expression) value is plotted for each control (green) and knockdown hairpin (blue denotes nominal p value < 0.01 by Mann-Whitney rank-sum test when comparing six gene-targeted hairpins with the control hairpins shown; gray denotes p > 0.01). Knockdown of *LRPPRC*, *SLIRP*, and *FASTKD4* caused the strongest depletion of *COX1*.

(B) Expression of the *rc_COX1* probe, which targets a noncoding region on the light strand, is plotted as in (A).

(C) The probe count for each knockdown hairpin is plotted for the *ND4* mRNA and *ND4_TRNH* junction probes. Genes that disproportionally affect one probe are found offset from the diagonal and labeled (Supplemental Experimental Procedures). Hairpins are colored based on knockdown strength (light blue for worst hairpin, blue for middle hairpin, dark blue for best hairpin, gray for no knockdown information, and green for control).

(D) The probe count for each knockdown shRNA hairpin is plotted for the *ND2* mRNA and *TRNM_ND2* junction probe as in (C).

See also Figure S3.

knocked down (Figure 2, C1), consistent with our expectation that depletion of both precursor and mature transcripts should reflect reduced transcription or mtDNA content. SLIRP and LRPPRC form a complex that is known to bind mtRNA and affect mt-mRNA levels (Mili and Piñol-Roma, 2003; Sasarman et al., 2010), but previous studies have both supported and contested a role for LRPPRC in transcription (Harmel et al., 2013; Sondheimer et al., 2010). Although all heavy-strand probes are impacted by *shLRPPRC* and *shSLIRP*, some junction probes are less strongly affected than the mRNA probes, suggesting a dual role for these regulatory proteins in posttranscriptional stabilization and transcription (Figure 1C). One theory consistent with our results is that the complex stabilizes the nascent transcript, as suggested elsewhere (Harmel et al., 2013). Because we could quantitate junction probes strand specifically, we were able to observe that *ND6* and most light-strand transcripts were unaffected by *LRPPRC* or *SLIRP* knockdown.

MitoString Highlights Distinct Regulatory Mechanisms for Coding and Noncoding Antisense Transcripts

Querying the MitoString compendium for specific transcripts, such as the heavy-strand mRNA *COX1*, uncovers distinct regulation for heavy-strand coding and light-strand noncoding RNAs. We identify nuclear genes whose knockdown alters *COX1* expression relative to the control hairpins, using a rank-sum statistic at a nominal p value < 0.01 (Figure 3A). On the left tail of the distribution, we recover the aforementioned *LRPPRC* and *SLIRP*. *COX1* is also depleted by knockdown of *FASTKD4* (also known as *TBRG4*), an uncharacterized protein that contains a RAP domain with predicted RNA-binding abilities

(Lee and Hong, 2004). Hairpins targeting the uncharacterized nucleoid component *DHX30* also deplete *COX1.* Interestingly, depletion of *SUPV3L1*, which is implicated in mtRNA degradation, also decreases *COX1* levels, possibly due to decreased mtDNA copy number, as described previously (Khidr et al., 2008). Silencing of *MTPAP* also diminishes *COX1* levels markedly, with the exception of one hairpin (Figure 3A). No knockdowns significantly increased *COX1* expression, perhaps due to its extremely high baseline abundance.

A similar analysis, focusing on the light-strand probe rc_COX1, reveals that the majority of significant knockdowns increase *rc_COX1* expression (Figure 3B). Since the noncoding portion of the light strand exists transiently, measuring these regions can identify degradation machinery. For the *rc_COX1* probe, knockdown of *SUPV3L1* induces a strong increase in transcript levels, confirming the role of *SUPV3L1* in this process (Figure 3B). However, *SUPV3L1* silencing actually decreases the level of some mt-mRNA transcripts, most notably *COX1*, *COX3*, and *ND4* (Figure 2, cluster C3), suggesting that its role in degradation may be selective. The response of *COX1* and *rc_COX1* transcripts to systematic RNAi perturbation highlights the distinct regulation of heavy-strand and light-strand transcripts shown in Figure 2.

Identifying Negative Regulators of mt-mRNA Abundance

We next sought to identify factors that function to repress the abundance of mt-mRNAs at steady state, in contrast to LRPPRC and SLIRP, which stabilize transcripts, by further mining our compendium. Loss of Mitochondrial GTPase 1 (*MTG1*) expression results in an increase of all mt-mRNAs except *ND5* (Figure S2D), and it is the second strongest-scoring gene on the right tail of the *COX1* distribution (Figure 3A). Although it is not significant when summarized by three hairpins for *COX1* individually (Figure 3A), measuring multiple genes results in an intriguing phenotype (Figure S2D). *MTG1* has been linked to respiration and translation in human cell lines, but up to now, the effect of *MTG1* knockdown on mt-mRNA levels had not been measured (Barrientos et al., 2003; Kotani et al., 2013). Knockdown of the uncharacterized gene *C21orf33* increases the mt-mRNAs *ND1-3*, with excellent knockdown-phenotype correlation, but has a minimal effect on the other transcripts (Figure S2E). In a complementary analysis using the GNF Mouse GeneAtlas (Lattin et al., 2008), we found that mRNA expression of the *C21orf33* mouse homolog is well correlated with nuclear-encoded OXPHOS gene expression (Figure S2F). Our data offer tantalizing clues, but more research is required to elucidate the exact roles of these genes.

Identifying Factors that Cleave Precursor Transcripts

A key advantage of the MitoString approach is that it simultaneously monitors both precursor and mature transcripts across a battery of perturbations, allowing identification of specific cleavage and processing factors. Within our data set, known cleavage factors form a distinct cluster marked by increased junction expression concomitant with stable mt-mRNA expression (Figure 2, cluster C3). These recently discovered factors include *MRPP1* and *MRPP2*, which encode subunits of the tRNA 5′ end cleavage machinery, and ELAC2, which cleaves the tRNA 3′ end (Brzezniak et al., 2011; Holzmann et al., 2008; Sanchez et al., 2011).

By comparing the abundance of specific mt-mRNAs with that of their unprocessed precursor, over all perturbations, we observe a background distribution from which outliers represent candidate cleavage factors (Figures 3C and 3D). The activity of mitochondrial RNase P is estimated by comparing the *ND4* transcript with its neighboring *ND4_TRNH* transcript (Figure 3C). If the junction is less efficiently cleaved, due to gene silencing, more unprocessed RNA will remain (Figure 3C). Hairpins targeting *MRPP1* and *MRPP2* have this effect and are consistently distinct from the background distribution in this case and in others tested (Figures 3C and S3A–S3C). We similarly investigate the 3′ cleavage site by comparing *ND2* counts with *TRNM_ND2* counts (Figure 3D). In this case, we identify *ELAC2*, *MRPP1*, and *MRPP2*, suggesting that knockdown of RNase P components can disrupt 3′ cleavage, as found previously for some junctions (Brzezniak et al., 2011; Sanchez et al., 2011).

We also interrogate junctions cleaved by noncanonical mechanisms. We find that silencing *MRPP1–MRPP3* or *ELAC2* does not influence the *ATP6/8_COX3* junction cleavage (Figures 2, cluster C3, and S3D–S3F). Further, outlier hairpins for this distribution are driven by mt-mRNA depletion, and not by *ATP6/8_COX3* transcript accumulation, leaving the cleavage factor for this junction unidentified (Figures S3D–S3F). The 5′ junction of *TRNQ* on the light strand abuts noncoding DNA and, unexpectedly, is more strongly affected by knockdown of *ELAC2* than by knockdown of *MRPP1/2* (Figure 2, cluster C3). Conversely, *TRNF_RNR1* is more strongly regulated by silencing of *MRPP1/2* and *SUPV3L1* than by silencing of *ELAC2*, although one *ELAC2* hairpin still has a strong effect (Figure 2, cluster C3). Both cases suggest noncanonical processing.

Impact of Known Disease Genes on mt-mRNA Levels

Our knockdown inventory includes 12 genes that have been implicated in Mendelian mitochondrial disease (Table S5). The disease genes *MTO1*, *PUS1*, and *TRMU* encode enzymes with well-established roles in tRNA modification and efficient translation, but to our knowledge, their role in regulating human mt-mRNA abundance has never been tested (Patton et al., 2005; Wang et al., 2010b; Yan and Guan, 2004; Zeharia et al., 2009). For the strongest *MTO1* knockdown hairpin (13% remaining), our compendium shows depletion of multiple mt-mRNAs (Figure 2), confirming similar findings in yeast (Wang et al., 2010b). Similarly, strong *PUS1* knockdown decreases *ATP6*, *COX3*, and *CYTB* mt-mRNA abundance (Figure 2). On the other hand, silencing of *TRMU* has a negligible effect on mt-mRNAs (Figure 2). In combination, these data suggest that some tRNA modifications may be necessary for proper mt-mRNA stability. The disease mechanisms may include both improper tRNA modification and mt-mRNA depletion.

Our compendium also expands our understanding of a number of other disease genes (Table S5). A mutation in *FASTKD2* has been implicated in COX deficiency (Ghezzi et al., 2008), and we now find a 2-fold decrease of *COX2/3*, *CYTB*, *ATP6/8*, and *ND3-4/4L-5* mt-mRNA expression under *FASTKD2* silencing by at least one hairpin (Figure 2). PNPT1, which has been implicated in both RNA degradation (Borowski et al., 2013) and

5S rRNA, *RNase P* RNA, and *MRP* RNA import (Wang et al., 2010a), was also recently associated with hearing loss and respiratory chain deficiency (Vedrenne et al., 2012; von Ameln et al., 2012). Our data reveal moderate increases in the short-lived transcripts *CYTB* and *ND2*, and moderate decreases in the long-lived transcripts *COX1–COX3* (Figure 2) in *PNPT1*-silenced cells, consistent with previous reports and highlighting the complexity of this protein's role in the cell (Borowski et al., 2013). Knockdown of TIMM8A, a known inner-mitochondrial-membrane translocase component that was targeted in the current study because it contains a zinc-finger-like motif, is correlated with moderately decreased mt-mRNA levels for almost all transcripts (Figure 2), and has been implicated in deafness-dystonia syndrome (Aguirre et al., 2006; Swerdlow et al., 2004).

Identifying Genes that Influence Mature mt-mRNA Abundance

To identify genes that specifically stabilize mature heavy-strand mt-mRNAs, we developed an ordered list that incorporates all of our heavy-strand probe data. We examined the ratio of the average heavy-strand mature mt-mRNA probes to the average heavy-strand precursor probes for each knockdown gene (Figure 4A). Using this measurement, we ordered each gene based on the rank sum of all hairpins targeting that gene (Figure 4A). This procedure is complementary to Figures 3C and 3D, which focus on two individual junctions. Proteins identified through this method might play a role in posttranscriptional processing, stability, and degradation.

POLRMT, which encodes the mtRNA polymerase, is among the highest-scoring hits, causing the ratio of mature mt-mRNA to precursor RNA to increase when silenced (Figure 4A). POLRMT has been well studied in vitro, but our study now perturbs it in vivo. This result suggests that when mtDNA transcription is reduced, the cell's response is to stabilize mature mt-mRNAs via an as yet uncharacterized regulatory mechanism.

A number of genes, when silenced, decrease the ratio of mt-mRNAs to precursor transcripts, suggesting that either the nascent strand is stabilized and/or the mt-mRNAs are destabilized. As expected, RNase P- and RNase Z-encoding genes (*MRPP1*, *MRPP2*, and *ELAC2*) are represented here because they stabilize nascent transcripts. Knockdown of an uncharacterized gene, *FASTKD4*, destabilizes mature transcripts and has an effect size similar to that produced by knockdown of known regulators (Figure 4A). *FASTKD4* clusters in our study with *MTPAP* and the ribosomal protein-encoding *MRPS17* (Figure 2, cluster C2). In general, silencing of genes in this cluster affects the mt-mRNA probes more strongly than the junction probes and does not affect all mt-mRNAs uniformly. Since FASTKD4 has not been previously linked to mt-mRNA expression, we pursued its function in more depth.

Silencing of *FASTKD4* Depletes Some, but Not All, mt-mRNAs

FASTKD4 belongs to a metazoan-specific cohort of proteins defined by the presence of FAST (Fas-activated serine/threonine kinase-like) and RAP (RNA-binding domain abundant in Apicomplexans) domains. The human genome encodes six of these proteins (FASTK and FASTKD1–FASTKD5), all of which localize to the mitochondrion (Simarro et al., 2010), although not all were identified in the initial MitoCarta compendium (Pagliarini et al., 2008). Mutations in *FASTKD2* are associated with COX deficiency (Ghezzi et al., 2008), and *FASTKD3* knockdown inhibits respiration in cultured cells (Simarro et al., 2010). *FASTK* encodes a kinase whose mitochondrial localization is disrupted during UV- or anti-Fas antibody-induced apoptosis (Li et al., 2004). FASTK also plays a role in alternative splicing in the nucleus, which requires the RAP domain (Izquierdo and Valcárcel, 2007; Simarro et al., 2007). Unlike FASTK, FASTKD4 does not have an identifiable kinase active site.

To confirm our screening result that *shFASTKD4* depletes a subset of mt-mRNAs, we began by validating the *FASTKD4* knockdown phenotype in an independent cell line (HEK293T). We used five distinct hairpins against *FASTKD4* and used MitoString to measure expression of the mitochondrial transcripts after 8 days of stable knockdown (Figure 4B). In agreement with our initial screen, only a subset of the mt-mRNA transcripts were affected (*COX1–COX3*, *ATP6/8*, *CYTB*, and *ND3*), and we found that mtDNA was actually increased, ruling out mtDNA depletion as a mechanism (Figure 4C). *ND1* was also consistently upregulated in both cases, whereas *ND2*, *ND4/4L*, and *ND5* remained unchanged. Thus, the impact of *FASTKD4* silencing on mt-mRNA abundance is robust across five distinct hairpin sequences and two cell lines. To confirm that this is an on-target effect of *FASTKD4* knockdown, we overexpressed a FLAG-tagged RNAi-resistant *FASTKD4* (*FASTKD4-FLAG*), as well as *FASTKD4* with four characteristic RAP domain residues mutated to alanines (*FASTKD4mut-FLAG*) (Figures 4D and 4E). *FASTKD4-FLAG* expression, but not *FASTKD4mut-FLAG* expression, is accompanied by recovery in RNA levels for affected transcripts (Figure 4E), proving that the *FASTKD4* knockdown is responsible for the observed phenotype.

We next used a complementary gene knockout strategy to perturb FASTKD4 and interrogate its impact on OXPHOS protein production. Although the knockdown produced a reliable RNA phenotype, residual FASTKD4 RNA was translated. We generated a *FASTKD4* knockout (*FASTKD4ko*) in HEK293T cells using the CRISPR/Cas9 system (Hsu et al., 2013), which enabled assays in the complete absence of FASTKD4. In our *FASTKD4ko* cell line, we identified three indels at the FASTKD4 locus that generated protein-terminating frameshifts, resulting in the absence of full-length protein (Figure 4F). In *FASTKD4ko*, we observed a reduced abundance of complex IV subunit COX2 protein that was rescued by *FASTKD4-FLAG* overexpression (Figures 4G and 4H). Complex I, II, III, and V nuclear subunits were unaffected, consistent with our screening results and the dependence of these complexes on mtDNA-encoded subunits (Figure 4H). Thus, two independent genetic strategies indicate that FASTKD4 is required for the proper expression of a specific subset of mtRNAs and, in the case of COX2, the protein product.

The Stability of a Subset of mtRNA Transcripts Requires FASTKD4

Assuming that all heavy-strand transcripts are transcribed concurrently, we hypothesized that the differential abundance of mt-mRNAs following silencing of *FASTKD4* is due to

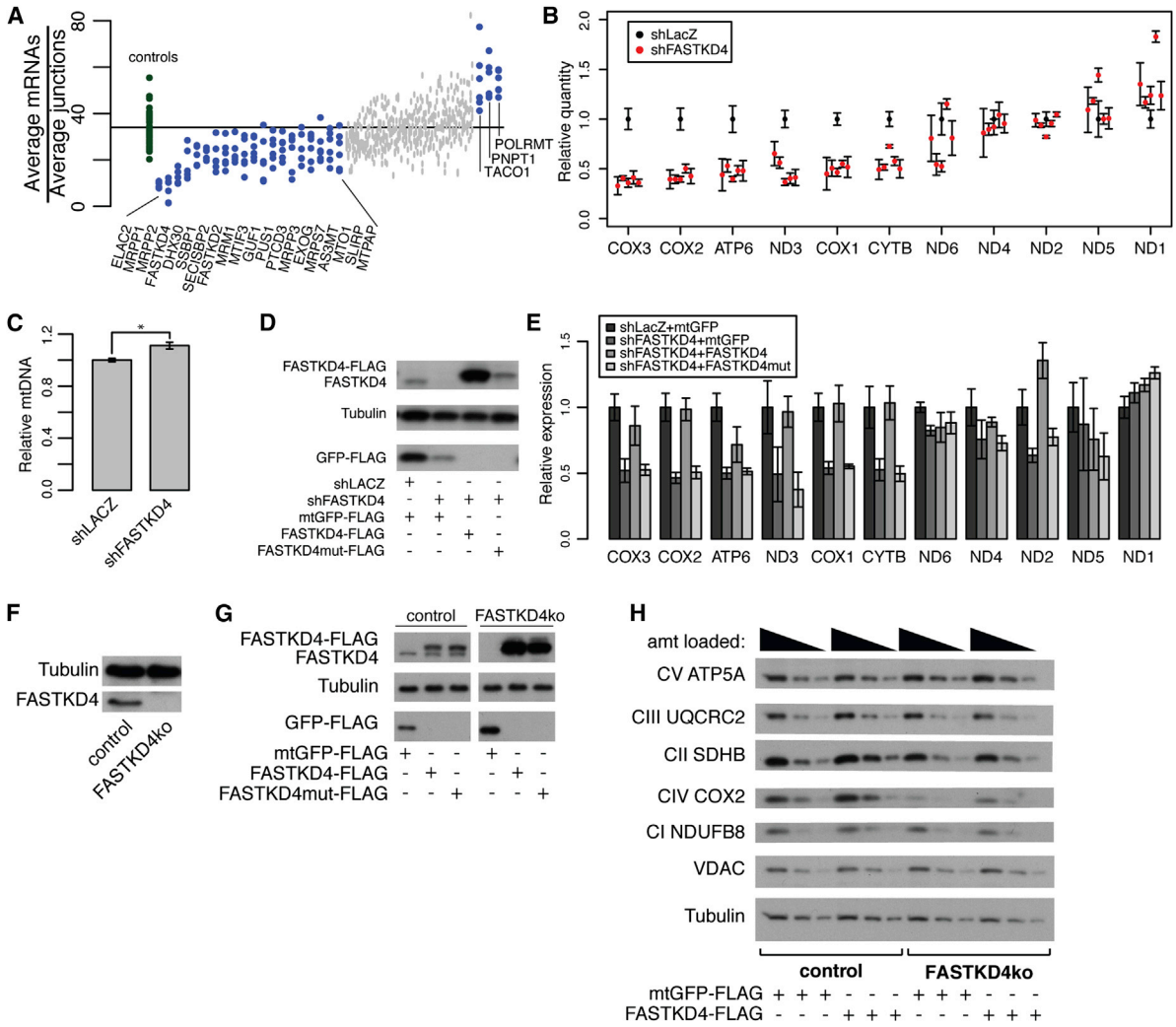

Figure 4. Loss of FASTKD4 Leads to Loss of a Subset of Steady-State mtDNA Gene Products

(A) The geometric mean of heavy-strand mRNA probe counts divided by the geometric mean of heavy-strand junction probe counts is plotted for each hairpin. Control hairpins are in green and knockdown hairpins are in blue or gray (blue represents nominal p value < 0.01 by Mann-Whitney rank-sum test).

(B) MitoString results normalized to *shLacZ* for five distinct *shFASTKD4* hairpins in HEK293T cells. Control hairpin is shown in black, *FASTKD4* hairpins are shown in red.

(C) Relative mtDNA content in *shLACZ* knockdown cells compared with *shFASTKD4* knockdown cells as measured by qPCR; *p < 0.05 (two-tailed unpaired t test).

(D) Western blot showing expression of FASTKD4-FLAG and FASTKD4 (detected by FASTKD4 antibody, top), tubulin (loading control, middle), and GFP-FLAG (overexpression control, bottom) in stable HEK293T cell lines. Cells are overexpressing RNAi-resistant *FASTKD4-FLAG* and *FASTKD4mut-FLAG* (with RAP domain point mutations) or *mitoGFP-FLAG* in the presence of *shLACZ* (control) or *shFASTKD4* knockdown, as indicated.

(E) Relative expression of each mt-mRNA probe quantified by MitoString, shown for the four cell lines depicted in (D).

(F) Western blot showing expression of FASTKD4 and tubulin in the *FASTKD4ko* CRISPR/Cas9 cell line.

(G) Western blot showing expression of FASTKD4-FLAG and FASTKD4 (detected by FASTKD4 antibody, top), tubulin (loading control, middle), and GFP-FLAG (overexpression control, bottom) in control and *FASTKD4ko* cell lines with overexpression of *FASTKD4-FLAG*, *FASTKD4mut-FLAG*, and *mtGFP-FLAG* as indicated (samples run on same gel with irrelevant lane removed).

(H) Western blot showing respiratory complex protein expression in control and *FASTKD4ko* cell lines, with *mtGFP-FLAG* or *FASTKD4-FLAG* overexpression as indicated. Three concentrations of each cell lysate were loaded as indicated. In all panels, error bars represent SEM, n = 3.

differential degradation rates. To measure RNA stability within the mitochondrion, we blocked POLRMT-mediated transcription with media containing a high concentration of ethidium bromide (ETBR) (Nagao et al., 2008). We quantitated the mt-mRNAs using qPCR following 6 hr of ETBR treatment, during which time period mitochondrial transcription was suspended. We determined the remaining fraction of RNA by comparing the ETBR-treated RNA with the untreated RNA. Of the six transcripts that were downregulated at steady state in FASTKD4 knockdown cells (Figure 4B), *COX2*, *ND3*, and *COX1* also showed a

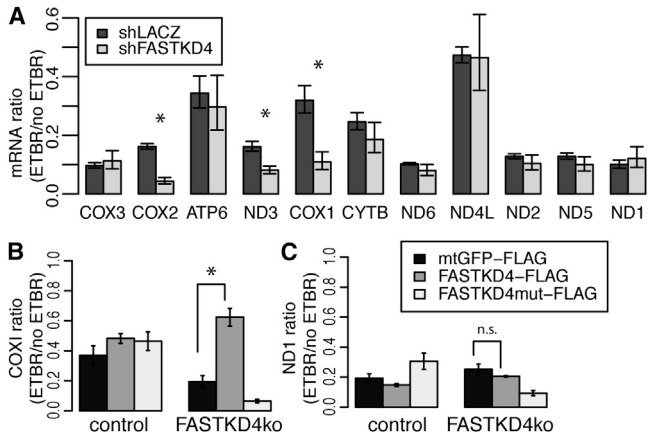

Figure 5. FASTKD4 Is Required for Stability of a Subset of mt-mRNAs

(A) The fraction of RNA that remained after ETBR transcription inhibition for 6 hr is plotted for each mt-mRNA as measured by qPCR in *shLACZ* and *shFASTKD4* cell lines.

(B and C) The fraction of remaining RNA is also plotted specifically for (B) *COX1* and (C) *ND1* in control or knockout cell lines expressing FLAG-tagged *mtGFP*, *FASTKD4*, and *FASTKD4mut*. Error bars represent SEM, n = 3. *p $\leq$ 0.05 (two-tailed unpaired t test).

strong decrease in the remaining fraction of RNA under ETBR treatment (Figure 5A), suggesting an increased degradation rate. *CYTB* also trended downward, but not significantly. The only transcripts that were depleted (Figure 4B) but not destabilized in our assay were *COX3* and *ATP6/8* (Figure 5A). Regulation of these two transcripts, which are part of the stable *ATP6/8_COX3* precursor, appears to be more complicated. By performing the same assay in our *FASTKD4ko*, we observed destabilized *COX1* and unchanged *ND1*, consistent with *shFASTKD4* (Figures 5B and 5C). Further, to rule out off-target RNAi effects, we rescued the *COX1* destabilization with *FASTKD4-FLAG* overexpression, but not with overexpression of *FASTKD4mut-FLAG* (Figure 5B).

FASTKD4 Associates with mtRNAs in the Matrix

We sought to define the suborganellar localization of FASTKD4 relative to the mt-mRNAs. FASTKD4, alongside soluble protein Cyclophilin D, was extractable with alkaline carbonate treatment of isolated mitochondria (Figure 6A). Additionally, FASTKD4 in mitoplasts was resistant to proteinase K treatment, alongside matrix protein Cyclophilin D (Figure 6A). All measured proteins were substrates for Proteinase K. Collectively, these studies indicate that FASTKD4 is a soluble protein that resides within the mitochondrial matrix.

Because FASTKD4 appears to stabilize mt-mRNAs, we investigated its binding to mtRNA by immunoprecipitating endogenous FASTKD4 from mitochondrial lysates and testing for mtRNA enrichment using qPCR. As controls, we immunoprecipitated TFAM, a known DNA-binding protein that is not expected to bind RNA, and LRPPRC, a known RNA-binding protein, alongside FASTKD4 in both wild-type and *FASTKD4ko* HEK293T cells (Figure 6B). In agreement with published results (Chujo et al., 2012; Sasarman et al., 2010), LRPPRC is associated with *COX1* mRNA (Figure 6C). In addition, LRPPRC associates with *12S* rRNA, but not nuclear *18S* rRNA (Figures 6D and 6E). In comparison, TFAM is not appreciably enriched for either RNA (Figures 6C and 6D). Similar to what is observed for LRPPRC, FASTKD4 immunoprecipitation enriches both *COX1* mRNA and *12S* rRNA, as compared with TFAM immunoprecipitation, in wild-type cells, but does not enrich nuclear *18S* rRNA (Figures 6C–6E). Intriguingly, FASTKD4 seems to bind *12S* almost as strongly as LRPPRC, but is a weaker binder of *COX1*. In *FASTKD4ko* cells, RNA enriched from FASTKD4 immunoprecipitation is indistinguishable from that enriched from TFAM and immunoglobulin G (IgG) immunoprecipitation. This proves that the RNA enrichment of *COX1* and *12S* rRNA is specifically due to FASTKD4 immunoprecipitation and is not an antibody artifact (Figures 6F–6H).

In addition to qPCR, we assessed our TFAM, FASTKD4, and LRPPRC immunoprecipitations with MitoString (Figures 6I and 6J). MitoString is valuable in this context because it allows strand-specific multiplexed measurement with a minimal sample. We found that the majority of heavy-strand abundant transcripts were enriched in both LRPPRC and FASTKD4 immunoprecipitations in comparison with TFAM immunoprecipitation (Figures 6I and 6J). In contrast, light-strand probes targeting *ND6* and light-strand intergenic space (*rc_ND5*, *rc_ND5_ND6*, and *rc_TRNQ_TRNM*) had less specific enrichment (Figure 6I). The heavy-strand junction probes spanning the *RNR2_TRNL1* junction and the *ATP6/8_COX3* junction were enriched in both FASTKD4 and LRPPRC immunoprecipitations. These results for LRPPRC are well correlated with previous findings obtained by qPCR (Chujo et al., 2012). In addition, our approach interrogates junction transcripts, especially on the light strand, that do not appear enriched relative to TFAM immunoprecipitation. *RNR2_TRNL1* is enriched in both LRPPRC and FASTKD4 immunoprecipitations at the same level as many of the mRNA genes. Our distinct approach and the inclusion of TFAM as a negative control demonstrate that FASTKD4 associates with mtRNAs, and further validate LRPPRC as an mtRNA-binding protein.

DISCUSSION

The expression of mtDNA requires nuclear-encoded proteins, yet at present we lack a full molecular description of this system. Previous approaches for measuring mtRNA, including northern blotting, qPCR, and next-generation sequencing, have been valuable but are limited by a lack of strand specificity or sample throughput. In the current study, we establish a facile assay, called MitoString, to systematically monitor precursor and mature mtRNA species following silencing of over 100 candidate nuclear-encoded factors. MitoString enables us to identify and classify mtRNA regulators based on their roles in transcription, cleavage, and stability. Through this compendium, we have expanded our understanding of previously characterized mtRNA processing proteins and implicated new players in this pathway, including the regulator FASTKD4.

Our approach, which measures both mature and precursor transcripts (Figure 1), implicates the LRPPRC-SLIRP complex in the production or stability of the heavy-strand precursor. Previous reports have implicated LRPPRC in promoting

transcription (Liu et al., 2011; Sondheimer et al., 2010) or the stability of individual mt-mRNAs (Chujo et al., 2012; Ruzzenente et al., 2012). We find that silencing of *SLIRP* or *LRPPRC* primarily affects the abundance of the heavy-strand precursor, indicating a role for the complex in either transcription or stabilization of the precursor (Figure 2). This decrease is accompanied by a more pronounced downregulation of mature heavy-strand mt-mRNAs, which may suggest a secondary role in mature transcript stability. In contrast, Gohil et al. (2010) measured precursors in *LRPPRC*-silenced cells by qPCR, which is not strand specific, and found no change in precursor abundance. Our method assesses just the heavy strand and reveals a 4-fold decrease in the same *TRNM_ND2* junction upon *LRPPRC* silencing (Figure 2). *LRPPRC* or *SLIRP* silencing has no effect on the light-strand mRNA *ND6* by our assay (Figure 2), consistent with strand-specific northern blot measurements (Ruzzenente et al., 2012) and in contrast to strand-insensitive qPCR results (Gohil et al., 2010). Recently, GRSF1 was implicated as a binder and regulator of *ND6* and its precursor strand, suggesting that a distinct mechanism operates on the light strand (Antonicka et al., 2013; Jourdain et al., 2013). Additionally, other investigators (Chujo et al., 2012) and we have found that LRPPRC binds heavy-strand transcripts with a higher abundance and specificity than light-strand transcripts, which is consistent with our steady-state mtRNA findings.

We confirm the role of proteinaceous RNase P in the cleavage of tRNA 5′ junctions and identify noncanonical cleavage sites. The MitoString profiles of RNase P subunits *MRPP1* and *MRPP2* knockdowns are well correlated, whereas the effect of *MRPP3* is weaker (Figures 2, 3C, and 3D). Our comprehensive approach builds on earlier findings focused on *MRPP1* and a subset of junctions (Holzmann et al., 2008), as well as work focused on *MRPP1 and MRPP3* (Sanchez et al., 2011). We also identify a few exceptions to this canonical cleavage process. On the light strand, *ELAC2* plays a role in the 5′ cleavage of *TRNQ*, which excises it from surrounding noncoding DNA (Figure 2, cluster C3). Also, *TRNF_RNR1*, which we expect to be regulated by ELAC2, is more strongly regulated by silencing of *MRPP1/2* and *SUPV3L1* (Figure 2, cluster C3). Consistent with this, this same *TRNF_RNR1* junction was previously reported to be unaffected by *ELAC2* small interfering RNA (siRNA) knockdown (Brzezniak et al., 2011). In a previous study, sequencing results suggested that knockdown of *ELAC2* and RNase P components did not affect all tRNA junctions (Sanchez et al., 2011). However, in all of our tested junctions on the heavy strand (excepting *ATP6/8_COX3*), either one or both of these components were involved (Figure 2). The discrepancy may stem from the prior study's exclusion of large precursor fragments due to size selection for tRNA-sized transcripts (Sanchez et al., 2011). Our assay revealed no obvious candidate for processing of the *ATP6/8_COX3* junction, as all outlier hairpins were driven by a decrease in mt-mRNA levels, not an increase in junction content (Figures S3D–S3F).

Although SUPV3L1 clearly plays a role in the degradation of light-strand transcripts, we find it has contrasting effects on different classes of mt-mRNAs (Figure 2). The short-lived *ND1* and *ND2* transcripts are increased, whereas the long-lived *COX1-3* transcripts are actually decreased, suggesting that SUPV3L1 may not be responsible for all degradation within the mitochondria. These contrasting effects were previously demonstrated (Szczesny et al., 2010), but only for a subset of mt-mRNAs. Here, we obtained data for all transcripts simultaneously. For the *TRNF_RNR1* and *TRNV_RNR2* junctions, which we expect to be a readout for transcriptional initiation, hairpins targeting *SUPV3L1* are the second-strongest inducers of expression (Figure 2, cluster C3). This increased transcription may pertain only to early-termination transcripts, which end after the second rRNA, since the *RNR2_TRNL1* junction and other heavy-strand junctions are not increased (Figure 2, cluster C3). Therefore, *SUPV3L1* depletion may increase ribosome production.

We find that FASTKD4 regulates a specific subset of mt-mRNAs. In general, *FASTKD4* silencing depletes transcripts that are long-lived while sparing the precursor strand (Figure 4B). The sole exceptions are *ND3*, a short-lived depleted transcript, and *ND4/4L*, a long-lived unaffected transcript. Most of the affected mt-mRNAs also have an increased degradation rate in both *FASTKD4* knockdown and knockout cells (Figures 5A and 5B). Thus, we hypothesize that FASTKD4 may serve to shield a specific set of mt-mRNAs from degradation by SUPV3L1 or an as yet unidentified degradation machinery. Unexpectedly, *ATP6* and *COX3* do not have an increased degradation rate by our assay (Figure 5A); however, the *ATP6/8_COX3* precursor is the sole mtDNA gene-gene junction and is relatively stable compared with other precursors, as estimated by probe counts. The factor responsible for *ATP6/8_COX3* cleavage remains undetermined and we expect that a full understanding of this mechanism will resolve the discrepancy we observe.

We cement a role for FASTKD4 in mtRNA metabolism based on the above findings, previous studies, and our immunoprecipitation of FASTKD4-associated mtRNA. FASTKD4 contains a RAP domain in common with experimentally validated RNA-binding proteins (Lee and Hong, 2004) and is found in a genome-wide mRNA-binding resource (Castello et al., 2012). Here, we show that FASTKD4 is localized to the mitochondrial matrix (Figure 6A) and associates with mtRNAs in a specific way (Figures 6C–6I). Our immunoprecipitation assay does not distinguish among the heavy-strand transcripts in terms of strength of association with FASTKD4, because this protein associates with all heavy-strand transcripts. However, mtRNA susceptibility to degradation may be influenced in part by the activity of another, as yet unidentified protein that requires FASTKD4 binding.

Why the mitochondrion maintains mt-mRNAs at such disparate levels is unknown, but we propose that it may provide a mechanism for ensuring proper OXPHOS complex stoichiometry. Across tissues, the molar ratios of different complexes are robust, but the mechanism that generates this stability is unknown (Benard et al., 2006). Complex I is consistently the least abundant among the OXPHOS complexes (Lenaz and Genova, 2010), and with the exception of the bicistronic *ND4/4L* transcript, mtDNA-encoded complex I transcripts have half-lives of <90 min (Nagao et al., 2008). In contrast, complexes IV and V are present at 3–12 times the concentration of complex I, a stoichiometry that we suggest could be metered in part by higher levels of complex IV and V component transcripts (*COX1-3* and *ATP6/8*),

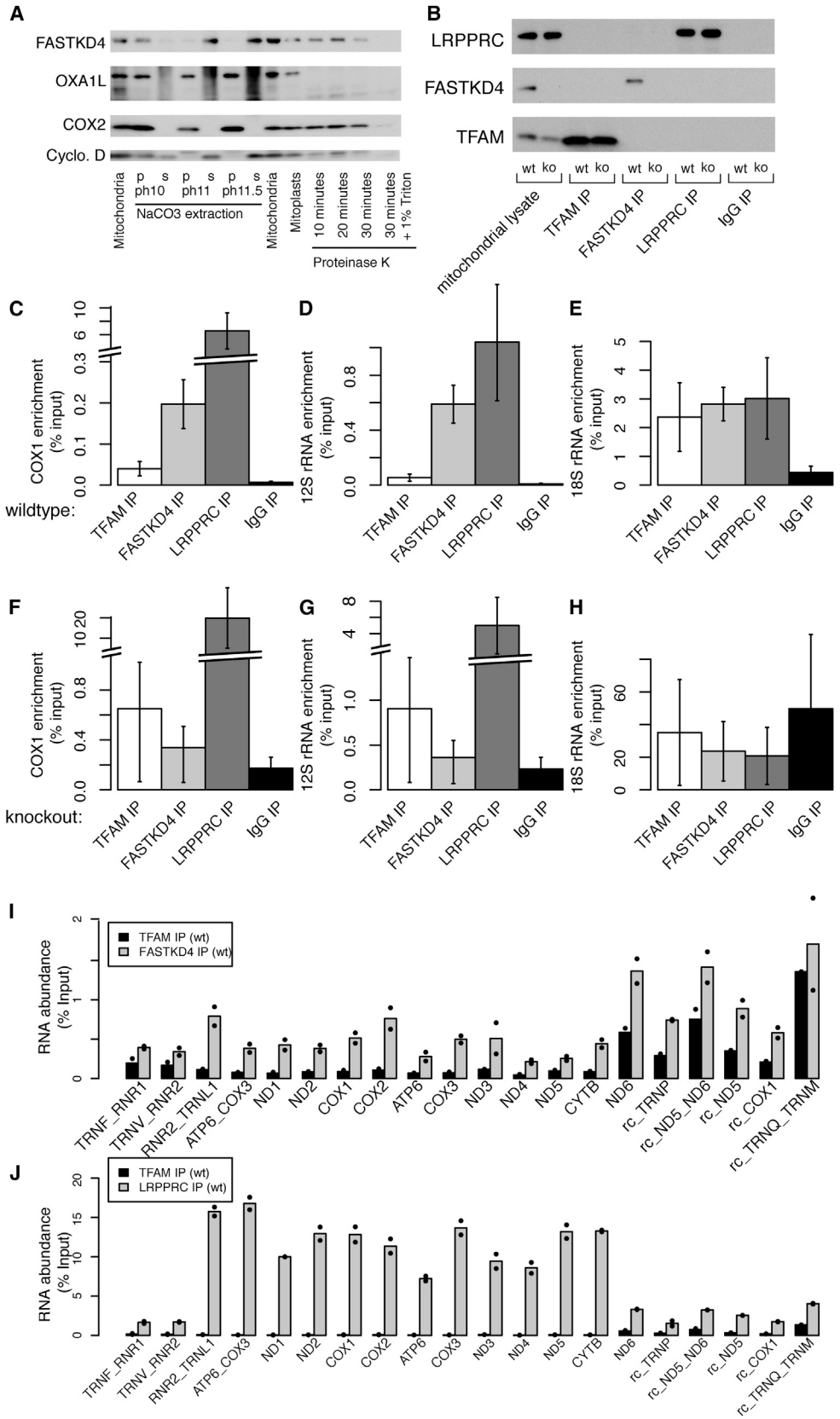

(legend on next page)

whose half-lives range from 138 to 231 min. Thus, the precise regulation of mt-mRNA transcript levels by factors such as FASTKD4 and SUPV3L1 may be important for ensuring proper OXPHOS complex stoichiometry and function.

We anticipate that in the future, MitoString may prove useful for interrogating the role of mt-mRNA processing directly in tissues from patients with mitochondrial disease. Our current study includes an analysis of 12 previously established disease genes (Table S5), three of which were previously linked to aberrant expression of mt-mRNAs in humans. Our current compendium demonstrates that *MTO1*, *PUS1*, and *FASTKD2* loss of function may also cause aberrant expression of mtRNAs. Our results point to additional modes of pathogenesis that may be at play in these disorders. As new genetic variants in mtRNA processing factors are identified in patients, a key challenge will be to prove their pathogenicity. MitoString is a highly quantitative and systematic approach for measuring mitochondrial gene expression that in principle can be easily applied to patient biopsy specimens. MitoString may therefore be a useful companion diagnostic for detecting aberrant expression of the mtDNA genome in human diseases.

EXPERIMENTAL PROCEDURES

Cell Culture

WI-38 fibroblasts and HEK293T cells were cultured in high-glucose Dulbecco's modified Eagle's medium (DMEM; Cat. No. 11995; Invitrogen) supplemented with 10% fetal bovine serum (Cat. No. F6178; Sigma) and 1× penicillin, streptomycin, and glutamine (Cat. No. 10378-016; Invitrogen) at 37°C with 5% CO_2.

Immunoblotting

Protein was electrophoresed on a 12% Novex Tris-glycine polyacrylamide gel at constant voltage (125 V). The gel was transferred to a polyvinylidene difluoride membrane (Trans-Blot Turbo Transfer System). Membranes were blocked for 1 hr at room temperature in Tris-buffered saline with 0.1% Tween-20 and 5% BSA (TBST-BSA). Membranes were incubated with primary antibody in TBST-BSA overnight at 4°C (Table S6). Secondary antibody was used at 1:5,000 for 1 hr at room temperature. Membranes were developed using WesternLightning Plus-ECL.

Screen

The three best hairpins per gene were selected, and then produced and arrayed by the RNAi Consortium (TRC) as previously described (Moffat et al., 2006).

WI-38 cells were seeded, infected after 24 hr, and selected 24 hr later. At 6 days postinfection, the cells were lysed with RLT buffer (Invitrogen) and β-mercaptoethanol (1:100), and frozen. RLT lysates were processed with a custom MitoString code set from NanoString Technologies per the manufacturer's instructions (Geiss et al., 2008). Screen details and data processing are described in Supplemental Experimental Procedures.

Protein Expression

plexFLAG was generated from plex-TRC-983 (TRC) by molecular cloning. pDONR223-FASTKD4 from a previously described cDNA library (Pagliarini et al., 2008) was mutagenized via QuikChange mutagenesis (Agilent) using the primers listed in Table S7. mtGFP was a gift from Y. Sancak. All cDNAs were cloned into plexFLAG via the Gateway system (Invitrogen).

Lentiviral Production and Infection

For follow-up experiments, shRNA lentiviral vectors (TRC) and FLAG-tagged expression constructs were used to produce virus and infect HEK293T cells as previously described (Baughman et al., 2009). For selection, 4 μg/ml puromycin or 5 μg/ml blasticidin was used.

mtDNA Quantitation

mtDNA quantification was performed as previously described (Baughman et al., 2009)

Mitochondrial Isolation, Na_2CO_3 Extraction, and Proteinase K Protection

HEK293T cells were suspended in isolation buffer (220 mM mannitol, 70 mM sucrose, 5 mM HEPES, 1 mM EGTA, pH 7.4 + cOmplete, EDTA-free Protease Inhibitor Cocktail [Roche]) and lysed using a cell disruption vessel (Parr Instrument) pressurized to 800 psi with nitrogen followed by homogenization with five strokes of a Teflon Potter Elvehjem homogenizer. Crude mitochondria were isolated by differential centrifugation at 600 *g* and 8,000 *g*. Mitoplasts were created by swelling with H_2O on ice and were stabilized in 137 mM KCl, 2.5 mM $MgCl_2$, 10 mM HEPES pH 7.2; pelleted at 8,000 *g*; and resuspended in isolation buffer. Na_2CO_3 extraction was performed on crude mitochondria, and proteinase K protection was performed on mitoplasts as previously described (Ryan et al., 2001).

Measurement of RNA Half-Lives

HEK293T cell lines were seeded the day before exposure to media with and without 1 μg/ml ETBR. After 6 hr, the cells were lysed with RLT (QIAGEN) for RNA extraction.

RNA Isolation and qPCR

RNA was isolated using the RNeasy protocol with DNase I treatment (QIAGEN). cDNA was transcribed using Superscript III First-Strand Synthesis Supermix (Invitrogen). qPCR was performed with a 7500-FAST ABI instrument and 2× Taqman FAST Advanced master-mix (Applied Biosystems) with mt-mRNA probes as described previously (Gohil et al., 2010).

RNA Immunoprecipitation

Isolated crude mitochondria were lysed in lysis buffer (50 mM HEPES [pH 7.4], 150 mM NaCl, 2 mM EDTA, 1% Triton, RNase Inhibitor). Lysates were treated with Turbo DNase for 1 hr at 37°C. After spinning at 16,000 *g* for 10 min at 4°C, the supernatant was precleared with Protein A agarose beads for 40 min at 4°C with rotation. The beads were spun out and the supernatant was incubated with antibody overnight at 4°C with rotation. Fresh Protein A agarose beads were blocked overnight with 1% BSA, 100 μg/ml heparin, and 100 μg/ml yeast tRNA in lysis buffer. The next day, the beads were washed three times with lysis buffer, added to the lysate-antibody mix, and incubated with rotation for 2 hr at 4°C. The bead complex was washed three times with lysis buffer

Figure 6. FASTKD4 Is Localized to the Matrix and Physically Associates with mtRNAs

(A) Western blot showing the presence of FASTKD4, OXA1L, COX2, and Cyclophilin D in isolated mitochondria, with carbonate extraction and with proteinase K digestion of mitoplasts.

(B) Western blot showing the presence of LRPPRC, FASTKD4, and TFAM after immunoprecipitation of each protein or IgG control in control (WT) and *FASTKD4ko* (KO) cells.

(C–E) qPCR was used to measure enrichment of (C) *COX1* mRNA, (D) *12S* rRNA, and (E) *18S* rRNA with immunoprecipitation of TFAM, FASTKD4, LRPPRC, and IgG from wild-type cells.

(F–H) qPCR-measured enrichment of transcripts measured in (C)–(E) under identical immunoprecipitation conditions, but in *FASTKD4ko* cells. Error bars represent SEM, n = 3.

(I) RNA abundance (% input) after FASTKD4 or TFAM immunoprecipitation in wild-type cells as measured by MitoString.

(J) RNA abundance (% input) after LRPPRC or TFAM immunoprecipitation in wild-type cells. Points represent each duplicate.

and three times with 500 mM NaCl lysis buffer. RNA samples were eluted with 300 μl 1 M $NaHCO_3$, 1% SDS at room temperature for 15 min. Beads were spun down and the supernatant was added to 12 μl 5 M NaCl. Then 700 μl of RLT buffer was added for RNA isolation. Protein samples were boiled in sample buffer for immunoblotting.

CRISPR Knockout Cell Line Generation

sgRNA and U6 primers (Table S7) were used to amplify the pX064 plasmid (a gift from F. Zhang) as previously described (Hsu et al., 2013). The PCR product was cotransfected with the Cas9 plasmid (a gift from F. Zhang) into HEK293T cells with XTreme Gene transfection reagent per the manufacturer's instructions. Cells were single-cell cloned and screened by western blot for FASTKD4 protein. The identified knockout was verified by PCR followed by subcloning and Sanger sequencing.

SUPPLEMENTAL INFORMATION

Supplemental Information includes Supplemental Experimental Experiments, three figures, and seven tables and can be found with this article online at http://dx.doi.org/10.1016/j.celrep.2014.03.035.

ACKNOWLEDGMENTS

We thank J. Baughman, X.R. Bao, S. Calvo, Y. Sancak, L. Strittmatter, I. Jain, N. Delaney, E. Kovacs-Bogdan, A. Li, S. Vafai, M. Staller, and N.M. Cabili for comments and helpful discussions. We thank the Broad Institute RNAi Platform for shRNA reagents, S. Silver and S. Gopal for advice, R. Boykin and G. Geiss of NanoString Technologies for technical assistance, and the Regev and Shamji groups for access to the nCounter analysis system. We thank M. Guttman, D. Shechner, J. Rinn, D. Scott, and F. Zhang for guidance on experimental protocols. This work was supported by an NSF graduate research fellowship to A.R.W. and an NIH grant (GM077465) to V.K.M.

Received: February 7, 2013
Revised: February 14, 2014
Accepted: March 11, 2014
Published: April 17, 2014

REFERENCES

Aguirre, L.A., del Castillo, I., Macaya, A., Medá, C., Villamar, M., Moreno-Pelayo, M.A., and Moreno, F. (2006). A novel mutation in the gene encoding TIMM8a, a component of the mitochondrial protein translocase complexes, in a Spanish familial case of deafness-dystonia (Mohr-Tranebjaerg) syndrome. Am. J. Med. Genet. A. *140*, 392–397.

Anderson, S., Bankier, A.T., Barrell, B.G., de Bruijn, M.H., Coulson, A.R., Drouin, J., Eperon, I.C., Nierlich, D.P., Roe, B.A., Sanger, F., et al. (1981). Sequence and organization of the human mitochondrial genome. Nature *290*, 457–465.

Antonicka, H., Sasarman, F., Nishimura, T., Paupe, V., and Shoubridge, E.A. (2013). The mitochondrial RNA-binding protein GRSF1 localizes to RNA granules and is required for posttranscriptional mitochondrial gene expression. Cell Metab. *17*, 386–398.

Barrientos, A., Korr, D., Barwell, K.J., Sjulsen, C., Gajewski, C.D., Manfredi, G., Ackerman, S., and Tzagoloff, A. (2003). MTG1 codes for a conserved protein required for mitochondrial translation. Mol. Biol. Cell *14*, 2292–2302.

Baughman, J.M., Nilsson, R., Gohil, V.M., Arlow, D.H., Gauhar, Z., and Mootha, V.K. (2009). A computational screen for regulators of oxidative phosphorylation implicates SLIRP in mitochondrial RNA homeostasis. PLoS Genet. *5*, e1000590.

Benard, G., Faustin, B., Passerieux, E., Galinier, A., Rocher, C., Bellance, N., Delage, J.P., Casteilla, L., Letellier, T., and Rossignol, R. (2006). Physiological diversity of mitochondrial oxidative phosphorylation. Am. J. Physiol. Cell Physiol. *291*, C1172–C1182.

Borowski, L.S., Dziembowski, A., Hejnowicz, M.S., Stepien, P.P., and Szczesny, R.J. (2013). Human mitochondrial RNA decay mediated by PNPase-hSuv3 complex takes place in distinct foci. Nucleic Acids Res. *41*, 1223–1240.

Brzezniak, L.K., Bijata, M., Szczesny, R.J., and Stepien, P.P. (2011). Involvement of human ELAC2 gene product in 3′ end processing of mitochondrial tRNAs. RNA Biol. *8*, 616–626.

Castello, A., Fischer, B., Eichelbaum, K., Horos, R., Beckmann, B.M., Strein, C., Davey, N.E., Humphreys, D.T., Preiss, T., Steinmetz, L.M., et al. (2012). Insights into RNA biology from an atlas of mammalian mRNA-binding proteins. Cell *149*, 1393–1406.

Chujo, T., Ohira, T., Sakaguchi, Y., Goshima, N., Nomura, N., Nagao, A., and Suzuki, T. (2012). LRPPRC/SLIRP suppresses PNPase-mediated mRNA decay and promotes polyadenylation in human mitochondria. Nucleic Acids Res. *40*, 8033–8047.

Finn, R.D., Tate, J., Mistry, J., Coggill, P.C., Sammut, S.J., Hotz, H.R., Ceric, G., Forslund, K., Eddy, S.R., Sonnhammer, E.L., and Bateman, A. (2008). The Pfam protein families database. Nucleic Acids Res. *36* (Database issue), D281–D288.

Geiss, G.K., Bumgarner, R.E., Birditt, B., Dahl, T., Dowidar, N., Dunaway, D.L., Fell, H.P., Ferree, S., George, R.D., Grogan, T., et al. (2008). Direct multiplexed measurement of gene expression with color-coded probe pairs. Nat. Biotechnol. *26*, 317–325.

Gelfand, R., and Attardi, G. (1981). Synthesis and turnover of mitochondrial ribonucleic acid in HeLa cells: the mature ribosomal and messenger ribonucleic acid species are metabolically unstable. Mol. Cell. Biol. *1*, 497–511.

Ghezzi, D., Saada, A., D'Adamo, P., Fernandez-Vizarra, E., Gasparini, P., Tiranti, V., Elpeleg, O., and Zeviani, M. (2008). FASTKD2 nonsense mutation in an infantile mitochondrial encephalomyopathy associated with cytochrome c oxidase deficiency. Am. J. Hum. Genet. *83*, 415–423.

Gohil, V.M., Nilsson, R., Belcher-Timme, C.A., Luo, B., Root, D.E., and Mootha, V.K. (2010). Mitochondrial and nuclear genomic responses to loss of LRPPRC expression. J. Biol. Chem. *285*, 13742–13747.

Harmel, J., Ruzzenente, B., Terzioglu, M., Spåhr, H., Falkenberg, M., and Larsson, N.G. (2013). The leucine-rich pentatricopeptide repeat-containing protein (LRPPRC) does not activate transcription in mammalian mitochondria. J. Biol. Chem. *288*, 15510–15519.

Holzmann, J., Frank, P., Löffler, E., Bennett, K.L., Gerner, C., and Rossmanith, W. (2008). RNase P without RNA: identification and functional reconstitution of the human mitochondrial tRNA processing enzyme. Cell *135*, 462–474.

Hsu, P.D., Scott, D.A., Weinstein, J.A., Ran, F.A., Konermann, S., Agarwala, V., Li, Y., Fine, E.J., Wu, X., Shalem, O., et al. (2013). DNA targeting specificity of RNA-guided Cas9 nucleases. Nat. Biotechnol. *31*, 827–832.

Izquierdo, J.M., and Valcárcel, J. (2007). Fas-activated serine/threonine kinase (FAST K) synergizes with TIA-1/TIAR proteins to regulate Fas alternative splicing. J. Biol. Chem. *282*, 1539–1543.

Jourdain, A.A., Koppen, M., Wydro, M., Rodley, C.D., Lightowlers, R.N., Chrzanowska-Lightowlers, Z.M., and Martinou, J.C. (2013). GRSF1 regulates RNA processing in mitochondrial RNA granules. Cell Metab. *17*, 399–410.

Khidr, L., Wu, G., Davila, A., Procaccio, V., Wallace, D., and Lee, W.H. (2008). Role of SUV3 helicase in maintaining mitochondrial homeostasis in human cells. J. Biol. Chem. *283*, 27064–27073.

Kotani, T., Akabane, S., Takeyasu, K., Ueda, T., and Takeuchi, N. (2013). Human G-proteins, ObgH1 and Mtg1, associate with the large mitochondrial ribosome subunit and are involved in translation and assembly of respiratory complexes. Nucleic Acids Res. *41*, 3713–3722.

Lattin, J.E., Schroder, K., Su, A.I., Walker, J.R., Zhang, J., Wiltshire, T., Saijo, K., Glass, C.K., Hume, D.A., Kellie, S., and Sweet, M.J. (2008). Expression analysis of G Protein-Coupled Receptors in mouse macrophages. Immunome Res. *4*, 5.

Lee, I., and Hong, W. (2004). RAP—a putative RNA-binding domain. Trends Biochem. Sci. *29*, 567–570.

Lenaz, G., and Genova, M.L. (2010). Structure and organization of mitochondrial respiratory complexes: a new understanding of an old subject. Antioxid. Redox Signal. *12*, 961–1008.

Li, W., Simarro, M., Kedersha, N., and Anderson, P. (2004). FAST is a survival protein that senses mitochondrial stress and modulates TIA-1-regulated changes in protein expression. Mol. Cell. Biol. *24*, 10718–10732.

Liu, L., Sanosaka, M., Lei, S., Bestwick, M.L., Frey, J.H., Jr., Surovtseva, Y.V., Shadel, G.S., and Cooper, M.P. (2011). LRP130 protein remodels mitochondria and stimulates fatty acid oxidation. J. Biol. Chem. *286*, 41253–41264.

Mercer, T.R., Neph, S., Dinger, M.E., Crawford, J., Smith, M.A., Shearwood, A.M., Haugen, E., Bracken, C.P., Rackham, O., Stamatoyannopoulos, J.A., et al. (2011). The human mitochondrial transcriptome. Cell *146*, 645–658.

Mili, S., and Piñol-Roma, S. (2003). LRP130, a pentatricopeptide motif protein with a noncanonical RNA-binding domain, is bound in vivo to mitochondrial and nuclear RNAs. Mol. Cell. Biol. *23*, 4972–4982.

Moffat, J., Grueneberg, D.A., Yang, X., Kim, S.Y., Kloepfer, A.M., Hinkle, G., Piqani, B., Eisenhaure, T.M., Luo, B., Grenier, J.K., et al. (2006). A lentiviral RNAi library for human and mouse genes applied to an arrayed viral high-content screen. Cell *124*, 1283–1298.

Nagao, A., Hino-Shigi, N., and Suzuki, T. (2008). Measuring mRNA decay in human mitochondria. Methods Enzymol. *447*, 489–499.

Ojala, D., Montoya, J., and Attardi, G. (1981). tRNA punctuation model of RNA processing in human mitochondria. Nature *290*, 470–474.

Pagliarini, D.J., Calvo, S.E., Chang, B., Sheth, S.A., Vafai, S.B., Ong, S.E., Walford, G.A., Sugiana, C., Boneh, A., Chen, W.K., et al. (2008). A mitochondrial protein compendium elucidates complex I disease biology. Cell *134*, 112–123.

Patton, J.R., Bykhovskaya, Y., Mengesha, E., Bertolotto, C., and Fischel-Ghodsian, N. (2005). Mitochondrial myopathy and sideroblastic anemia (MLASA): missense mutation in the pseudouridine synthase 1 (PUS1) gene is associated with the loss of tRNA pseudouridylation. J. Biol. Chem. *280*, 19823–19828.

Piechota, J., Tomecki, R., Gewartowski, K., Szczesny, R., Dmochowska, A., Kudła, M., Dybczyńska, L., Stepien, P.P., and Bartnik, E. (2006). Differential stability of mitochondrial mRNA in HeLa cells. Acta Biochim. Pol. *53*, 157–168.

Puranam, R.S., and Attardi, G. (2001). The RNase P associated with HeLa cell mitochondria contains an essential RNA component identical in sequence to that of the nuclear RNase P. Mol. Cell. Biol. *21*, 548–561.

Ruzzenente, B., Metodiev, M.D., Wredenberg, A., Bratic, A., Park, C.B., Cámara, Y., Milenkovic, D., Zickermann, V., Wibom, R., Hultenby, K., et al. (2012). LRPPRC is necessary for polyadenylation and coordination of translation of mitochondrial mRNAs. EMBO J. *31*, 443–456.

Ryan, M.T., Voos, W., and Pfanner, N. (2001). Assaying protein import into mitochondria. Methods Cell Biol. *65*, 189–215.

Sanchez, M.I., Mercer, T.R., Davies, S.M.K., Shearwood, A.M., Nygård, K.K.A., Richman, T.R., Mattick, J.S., Rackham, O., and Filipovska, A. (2011). RNA processing in human mitochondria. Cell Cycle *10*, 2904–2916.

Sasarman, F., Brunel-Guitton, C., Antonicka, H., Wai, T., and Shoubridge, E.A.; LSFC Consortium (2010). LRPPRC and SLIRP interact in a ribonucleoprotein complex that regulates posttranscriptional gene expression in mitochondria. Mol. Biol. Cell *21*, 1315–1323.

Scarpulla, R.C., Vega, R.B., and Kelly, D.P. (2012). Transcriptional integration of mitochondrial biogenesis. Trends Endocrinol. Metab. *23*, 459–466.

Simarro, M., Mauger, D., Rhee, K., Pujana, M.A., Kedersha, N.L., Yamasaki, S., Cusick, M.E., Vidal, M., Garcia-Blanco, M.A., and Anderson, P. (2007). Fas-activated serine/threonine phosphoprotein (FAST) is a regulator of alternative splicing. Proc. Natl. Acad. Sci. USA *104*, 11370–11375.

Simarro, M., Gimenez-Cassina, A., Kedersha, N., Lazaro, J.B., Adelmant, G.O., Marto, J.A., Rhee, K., Tisdale, S., Danial, N., Benarafa, C., et al. (2010). Fast kinase domain-containing protein 3 is a mitochondrial protein essential for cellular respiration. Biochem. Biophys. Res. Commun. *401*, 440–446.

Sondheimer, N., Fang, J.-K., Polyak, E., Falk, M.J., and Avadhani, N.G. (2010). Leucine-rich pentatricopeptide-repeat containing protein regulates mitochondrial transcription. Biochemistry *49*, 7467–7473.

Swerdlow, R.H., Juel, V.C., and Wooten, G.F. (2004). Dystonia with and without deafness is caused by TIMM8A mutation. Adv. Neurol. *94*, 147–154.

Szczesny, R.J., Borowski, L.S., Brzezniak, L.K., Dmochowska, A., Gewartowski, K., Bartnik, E., and Stepien, P.P. (2010). Human mitochondrial RNA turnover caught in flagranti: involvement of hSuv3p helicase in RNA surveillance. Nucleic Acids Res. *38*, 279–298.

Vedrenne, V., Gowher, A., De Lonlay, P., Nitschke, P., Serre, V., Boddaert, N., Altuzarra, C., Mager-Heckel, A.M., Chretien, F., Entelis, N., et al. (2012). Mutation in PNPT1, which encodes a polyribonucleotide nucleotidyltransferase, impairs RNA import into mitochondria and causes respiratory-chain deficiency. Am. J. Hum. Genet. *91*, 912–918.

von Ameln, S., Wang, G., Boulouiz, R., Rutherford, M.A., Smith, G.M., Li, Y., Pogoda, H.M., Nürnberg, G., Stiller, B., Volk, A.E., et al. (2012). A mutation in PNPT1, encoding mitochondrial-RNA-import protein PNPase, causes hereditary hearing loss. Am. J. Hum. Genet. *91*, 919–927.

Wagner, B.K., Kitami, T., Gilbert, T.J., Peck, D., Ramanathan, A., Schreiber, S.L., Golub, T.R., and Mootha, V.K. (2008). Large-scale chemical dissection of mitochondrial function. Nat. Biotechnol. *26*, 343–351.

Wang, G., Chen, H.W., Oktay, Y., Zhang, J., Allen, E.L., Smith, G.M., Fan, K.C., Hong, J.S., French, S.W., McCaffery, J.M., et al. (2010a). PNPASE regulates RNA import into mitochondria. Cell *142*, 456–467.

Wang, X., Yan, Q., and Guan, M.X. (2010b). Combination of the loss of cmnm5U34 with the lack of s2U34 modifications of tRNALys, tRNAGlu, and tRNAGln altered mitochondrial biogenesis and respiration. J. Mol. Biol. *395*, 1038–1048.

Yan, Q., and Guan, M.X. (2004). Identification and characterization of mouse TRMU gene encoding the mitochondrial 5-methylaminomethyl-2-thiouridylate-methyltransferase. Biochim. Biophys. Acta *1676*, 119–126.

Zeharia, A., Shaag, A., Pappo, O., Mager-Heckel, A.M., Saada, A., Beinat, M., Karicheva, O., Mandel, H., Ofek, N., Segel, R., et al. (2009). Acute infantile liver failure due to mutations in the TRMU gene. Am. J. Hum. Genet. *85*, 401–407.